

Measurement of electromagnetic radiation force using a capacitance interferometer

Devashish Shah,* Pradumn Kumar, and Pradeep Sarin

Department of Physics, Indian Institute of Technology Bombay, Powai, Mumbai 400076 India

(Dated: August 12, 2024)

Interferometry forms the cornerstone of several high-precision sensing techniques in physics. We present a mechanical cantilever-based tabletop interferometer to measure the force exerted by light from a pulsed laser beam. The experiment uses the interference of two sinusoidal voltage signals passing through nominally similar dielectrics formed by two cantilever-based air capacitors on a PCB. The radiation force exerted by a pulsed laser beam on one of the air capacitors causes a change in its capacitance, which is measured as a proportional change in the interfering voltage signal. This experiment uses equipment commonly found in an undergraduate teaching laboratory for physics and electronics while providing excellent insight into electromagnetic wave theory, circuit design for low-noise measurements, Fourier analysis, and interpretation of experimental data.

I. INTRODUCTION

Students typically learn about electromagnetic radiation, radiation momentum-density, and radiation force in advanced courses on electromagnetism (EM). Often, this remains a purely theoretical concept. Historically, it has been difficult to unambiguously measure the effect of radiation force on macroscopic objects.^{1,2} In recent years, several measurements of the effects of radiation force have been made using micromachined resonators^{3,4} and precision optics.⁵ We present a novel experiment to determine the radiation force exerted by a pulsed laser source on a thin metal strip suspended over a PCB trace in ambient air. The experiment can be performed using equipment typically found in an undergraduate teaching laboratory.

Following the notation of D.J. Griffiths,⁶ the momentum density of an EM wave $\{\vec{E}(\vec{x}, t), \vec{B}(\vec{x}, t)\}$ in free space is:

$$\vec{P}_{rad} = \epsilon_0(\vec{E} \times \vec{B}) = \frac{1}{c^2} \vec{S}, \quad (1)$$

where $\vec{S} = (\vec{E} \times \vec{B})/\mu_0$ is the Poynting vector, with μ_0 and ϵ_0 being the permeability and permittivity of free space respectively. For a plane EM wave $\vec{E} = E_0 \cos(kx - \omega t)\hat{z}$ incident normally on a surface with area \mathcal{A} , the radiation force is:⁷

$$F_{rad} = \frac{I\mathcal{A}}{c}(2r(\lambda) + a(\lambda)). \quad (2)$$

Here, I is the time-averaged intensity $c\epsilon_0 E_0^2/2$. The incident light is partly absorbed and reflected for a real material with associated absorption and reflection coefficients, $a(\lambda)$ and $r(\lambda)$, which are wavelength-dependent.

For a typical lab-grade laser power of 1W, we expect the radiation force to be $\mathcal{O}(\text{nN})$, which we intend to measure. To this end, Section II describes the circuit theory and cantilever dynamics forming the basis of the experiment. Section III describes the experimental setup, followed by results and analysis in Section IV. Analytical calculations for the flexure of a cantilever are provided in Appendix A.

II. CIRCUIT THEORY AND CANTILEVER DYNAMICS

The device under test (DUT) is a thin brass strip in parallel to a copper PCB trace, forming an air capacitor C_{DUT} (Fig. 1a). One end of the strip is soldered to the input signal node V_{DUT} . C_{DUT} is in series with a reference air capacitor C_{Ref} , formed using a similar metal strip soldered to a signal trace V_{Ref} . The metal strip for C_{Ref} is kept shorter and broader to keep it rigid and fixed. These capacitors are placed in the path of sinusoidal signals forming the ‘‘capacitance bridge.’’ C_{G1} is the lumped parasitic capacitance to ground at the node V_{Bridge} (Fig. 1b).

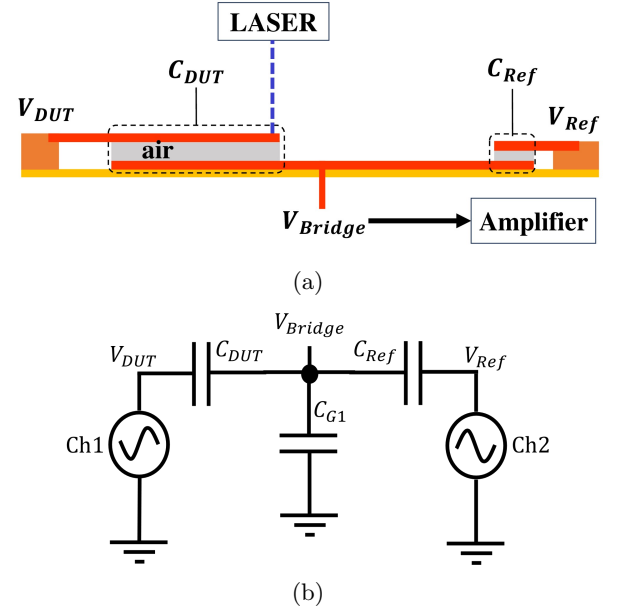


FIG. 1: (a) Schematic of the physical bridge circuit made of two air capacitors. (b) Capacitance bridge circuit.

The signals fed at one node of each of the two bridge capacitors are sinusoidal voltages $V_{DUT} \sin(\omega_0 t)$ and $V_{Ref} \sin(\omega_0 t + \eta)$ with adjustable amplitudes, frequency, and relative phase (η), generated using a two-channel

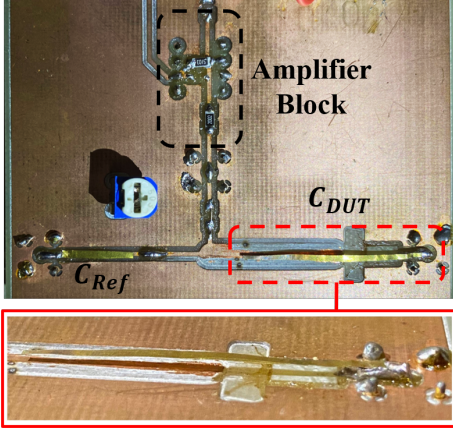


FIG. 2: Image of the assembled PCB with the bridge circuit and an integrated Op-Amp (LF411C) based inverting amplifier. Inset: zoomed-in image of C_{DUT} .

function generator. In principle, a single true floating differential sinusoidal voltage can be used if $C_{Ref} = C_{DUT}$. During measurement, the phase is adjusted such that the two signals are exactly out of phase ($\eta = \pi$). The result of the destructively interfering sinusoidal signals is seen at the junction labeled V_{Bridge} in the figure.

When the amplitudes, V_{Ref} and V_{DUT} are adjusted such that V_{Bridge} is zero, The bridge is said to be "balanced." In that case, the ratio of voltage amplitudes is simply related to the inverse ratio of associated capacitances. Using Kirchoff's current and voltage laws for the circuit in Fig. 1b:

$$C_T V_{Bridge} = C_{DUT} V_{DUT} - C_{ref} V_{Ref}. \quad (3)$$

Here, $C_T = C_{DUT} + C_{Ref} + C_{G1}$ is the combined capacitance. The negative sign for the second term arises due to the π phase offset. For $V_{Bridge} = 0$, we get:

$$V_{DUT} = V_{Ref} \frac{C_{Ref}}{C_{DUT}}. \quad (4)$$

Consequently, the differential of Eq. (3) gives:

$$\Delta V_{Bridge} = \frac{\Delta C_{DUT}}{C_T} V_{DUT}. \quad (5)$$

When the bridge is balanced (or nearly so), any change in the cantilever capacitance ΔC_{DUT} reflects as a proportional change in bridge voltage amplitude ΔV_{Bridge} . In practice, V_{Bridge} is amplified using an amplifier integrated into the PCB (Fig. 2), which we measure as V_{Out} .

The cantilever acts as a springy diving board. When hit by a focused laser pulse, it springs back and forth, changing the air gap, and hence C_{DUT} . ΔC_{DUT} is large when the pulsing of the laser is resonant with the cantilever's natural frequency. The change in the capacitance is estimated to calculate the force exerted by light on the cantilever.

Analogous to any linear damped-driven oscillator, the deflection of the cantilever in the presence of an external

drive can be described as a superposition of eigenmodes ($\phi_i e^{i\omega_i t}$) with associated natural frequencies ($\omega_i = 2\pi f_i$). Fig. 3 shows the spatial profile of the first three flexural eigenmodes. A theoretical estimate of the first harmonic

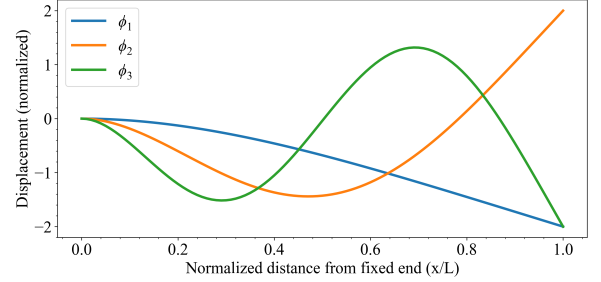


FIG. 3: The first three flexural eigenmodes of an ideal cantilever.

frequency of the flexure of an ideal cantilever can be made following the analysis shown in the Appendix A. For a brass cantilever with Young's modulus $E = (1.0 \pm 0.1) \cdot 10^{11} \text{ N/m}^2$, density $\rho = 7575 \pm 19.9 \text{ kg/m}^3$, length $L_C = 2.740 \pm 0.002 \text{ cm}$, width $b = 1.00 \pm 0.02 \text{ mm}$, and thickness $h = 50 \mu\text{m}$, the first natural frequency is:

$$\begin{aligned} f_1^{theory} &= \frac{1}{2\pi} \omega_1 = \frac{1.875^2}{2\pi} \cdot \left(\frac{EI}{\rho AL_C^4} \right)^{\frac{1}{2}} \\ &= \mathbf{40.25 \pm 2.93 \text{ Hz}}. \end{aligned} \quad (6)$$

The density of the brass sheet ($h = 50 \mu\text{m}$) used is calculated from the mass measured for $3.4 \times 0.98 \text{ cm}^2$ piece using a *Sartorius BT 224 S* Balance. Here, we account for a large error in E , which depends on the exact proportion of metals in the alloy. Dimensions L_C and b of the cantilever (DUT) are measured using a Vernier Caliper accurate up to 0.02 mm.

III. EXPERIMENTAL SETUP

A. PCB and Laser setup

The V_{Out} port is used to measure the final amplified signal during the experiment. In practice, $V_{Bridge}(t) \sin(\omega_0 t)$ is amplified using an inverting amplifier, giving $V_{Out}(t) \sin(\omega_0 t + \delta)$. The time dependence in the amplitudes (envelopes) V_{Bridge} and V_{Out} are directly correlated to $\Delta C_{DUT}(t)$. δ , the phase introduced due to the finite delays in the Op-Amp circuit doesn't affect the analysis. We used LEMO connectors (Fig. 4a) because of their compact size compared to BNC connectors, which keeps the PCB assembly small and easy to align. High-quality equal-length (1m) coaxial cables were used to minimize stray capacitance and phase delays in the signal paths. The inverting voltage amplifier built using an LF411C (Texas Instruments)⁸ JFET input Op-Amp IC has a feedback ratio of $510 \text{ k}\Omega / 20 \text{ k}\Omega$ and is powered using

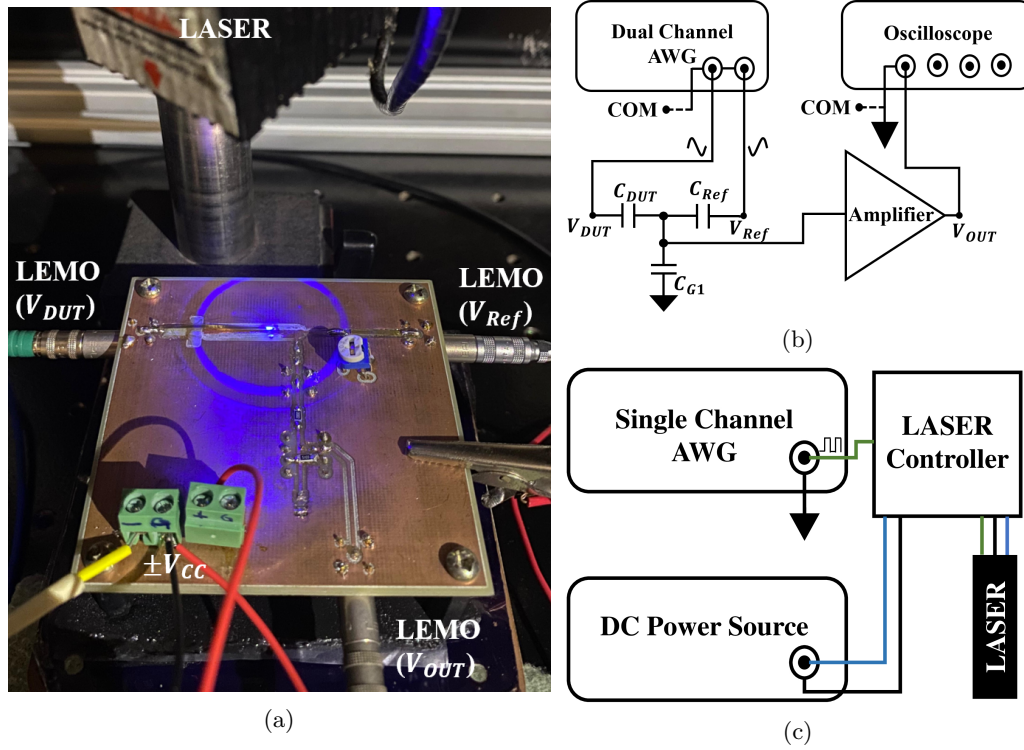


FIG. 4: (a) Experimental setup with the LASER focused on the tip of C_{DUT} , (b) schematic of the experimental setup, and (c) a schematic of the laser setup.

two 9V batteries. 222.1 kHz out-of-phase sinusoidal signals are sourced as V_{DUT} and V_{Ref} using a two-channel function generator (Fig. 4b). All signals are read out on a *LeCroy 8254M Digital Oscilloscope* with a 40 GS/s maximum sampling rate. The PCB is aligned on a horizontal x-y plane placed on a rubber pad for vibration isolation. It is essential to perform the experiment in the absence of air currents that may affect the cantilever. Thus, the setup is enclosed in a large cabinet, which also protects the eyes from the scattered laser light.

We use a blue ($\lambda = 450$ nm) laser with an RMS optical power measured to be $\mathbf{P_{RMS} = 0.4 \pm 0.02$ mW} using a *Coherent 200* laser power meter when the laser is driven by a 50% duty cycle digital signal. This type of laser is commonly used in laser engraving machines and is popular with DIY enthusiasts. The laser is controlled by a current drive circuit using a two-level digital pulse input (voltage V_L switching between 0 V and 5 V) with variable duty cycle and frequency (f_L). The drive frequency for this model can be varied from DC up to 2 kHz, giving us a broad range of frequencies at which the cantilever can be driven. This square wave digital pulse with variable frequency and duty cycle is generated using a single channel function generator (Fig. 4c). The laser is mounted on a clamp with adjustable z-alignment, and the height is adjusted such that the beam has the smallest spot size (≤ 0.25 mm²) when focused on the tip of the cantilever (Fig. 4a).

B. Amplifier gain and capacitance values

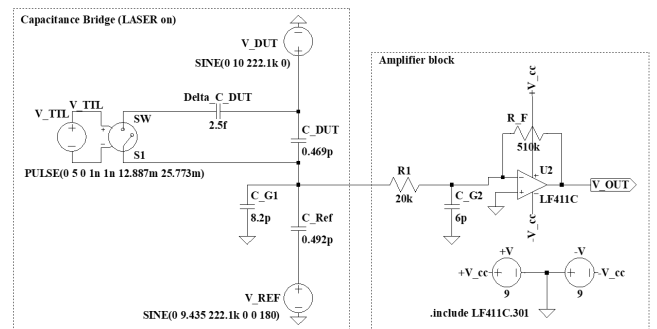
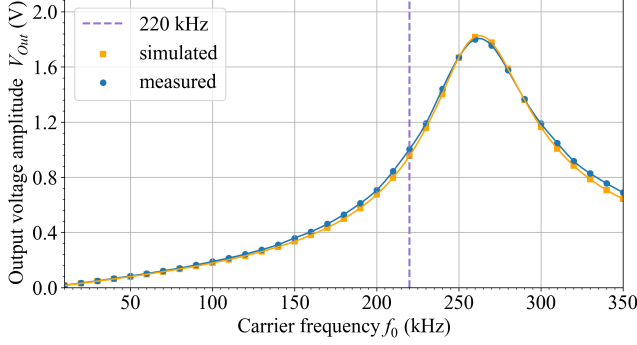


FIG. 5: LTSpice circuit for simulations.

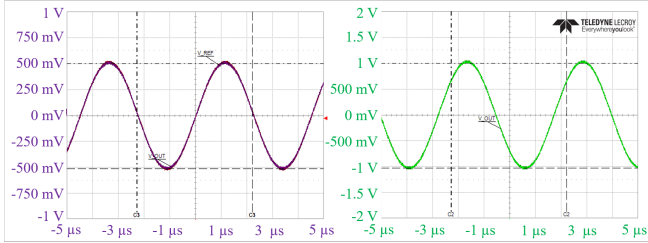
The electronic circuit can be divided into two blocks, namely, the capacitance bridge and the amplifier block (Fig. 5). The capacitances C_{Ref} , C_{DUT} , and C_{G1} for the bridge circuit are measured to be $\mathbf{0.492 \pm 0.01$ pF, $\mathbf{0.467 \pm 0.01$ pF, and $\mathbf{8.2 \pm 0.1}$ pF using a *Boonton 7200* capacitance meter. Due to the capacitive nature of the input to the inverting amplifier, the gain of the amplifier varies strongly with the carrier frequency (f_0), showing a peak at $\simeq 260$ kHz. The profile of the gain curve is measured experimentally by applying 1 V_{pp} (peak to peak value) in-phase sinusoidal signals with amplitudes $V_{DUT} = V_{Ref} = V_{In}$ and measuring V_{Out} at frequencies

from 10kHz up to 350kHz. We choose $f_0 = 222.1$ kHz as the operating frequency where V_{Out}/V_{In} is 2.

LTSpice⁹ simulations are used to understand and verify experimentally measured results. C_{G2} is the effective lumped parasitic capacitance seen between the two input terminals of the Op-Amp, which cannot be measured in situ. Simulating and matching the gain curves allows for the determination of $C_{G2} = 6.0$ pF (Fig. 6a). Identical to the experiment, we simulate the gain curve by using in-phase sinusoidal signals with amplitudes $V_{DUT} = V_{Ref} = 1$ V_{pp} (with $\Delta C_{DUT} = 0$), and performing a frequency sweep in LTSpice.



(a)



(b)

FIG. 6: (a) Gain curve ($V_{Ref} = V_{DUT} = 1$ V_{pp}): measured (\square) and simulated (\circ) values. (b) Gain Measurement at the operating frequency $f_0 = 222.1$ kHz: left panel shows applied $V_{DUT} = V_{Ref}$ and right panel is the measured V_{Out} .

C. Steady state calibration

The first step while setting up the experiment is to “balance” the capacitance bridge (Fig. 7). This is done by applying out-of-phase sinusoidal voltages at frequency $f_0 = 222.1$ kHz with $V_{DUT} = 20$ V_{pp} and varying V_{Ref} until the amplitude V_{Out} is minimized. Ideally, for exact destructive interference V_{Bridge} should be zero. A small residual phase difference due to the minimum 1° least count of the AFG causes a residual V_{Out} . We observe $V_{Ref} = 19$ V_{pp} balances the bridge ($V_{Out} \simeq 120$ mV_{pp}). Thus, Eq. (4) gives $C_{DUT}/C_{Ref} = V_{Ref}/V_{DUT} = 0.95$. This is in agree-

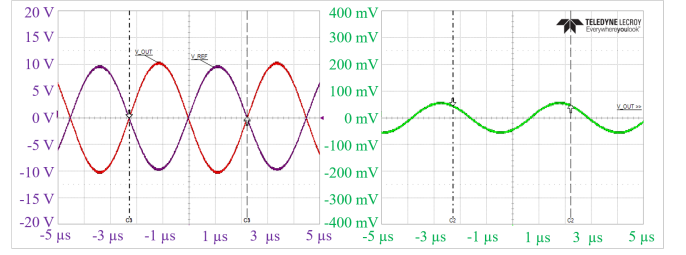
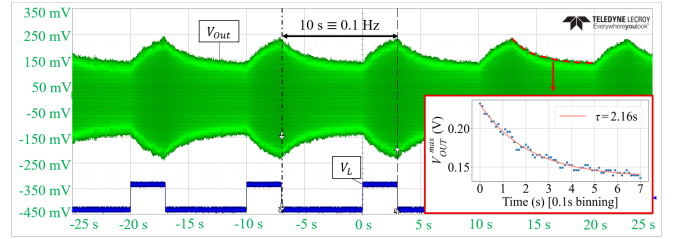


FIG. 7: Oscilloscope data for the balanced bridge: $V_{Ref} = 19$ V_{pp} (left panel), $V_{DUT} = 20$ V_{pp} (left panel), and $V_{Out} = 120$ mV_{pp} (right panel).

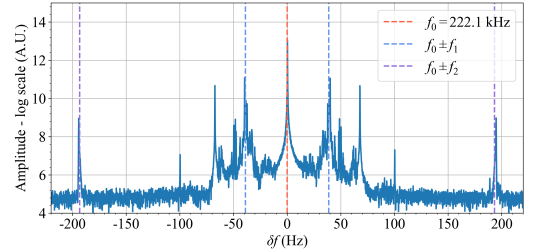
ment with the measured values of bridge capacitances, where $C_{DUT}/C_{Ref} = 0.949 \pm 0.004$. The carrier frequency f_0 and signal amplitudes V_{Ref} and V_{DUT} are kept constant for all further measurements.

IV. RESULTS AND ANALYSIS

A. Determination of cantilever resonant frequencies



(a)



(b)

FIG. 8: (a) Cantilever response for an off-resonance excitation at $f_L = 0.1$ Hz. Inset: exponential fit to the envelope to extract damping constant τ . (b) Discrete Fourier transform of V_{Out} showing frequencies of resonant modes.

To characterize the dynamics of the cantilever, C_{DUT} is excited using a $f_L = 0.1$ Hz and 30% duty cycle laser pulse. This measurement allows for the estimation of the damping constant and gives an estimate of the natural frequencies. Since f_L is much lower than the expected

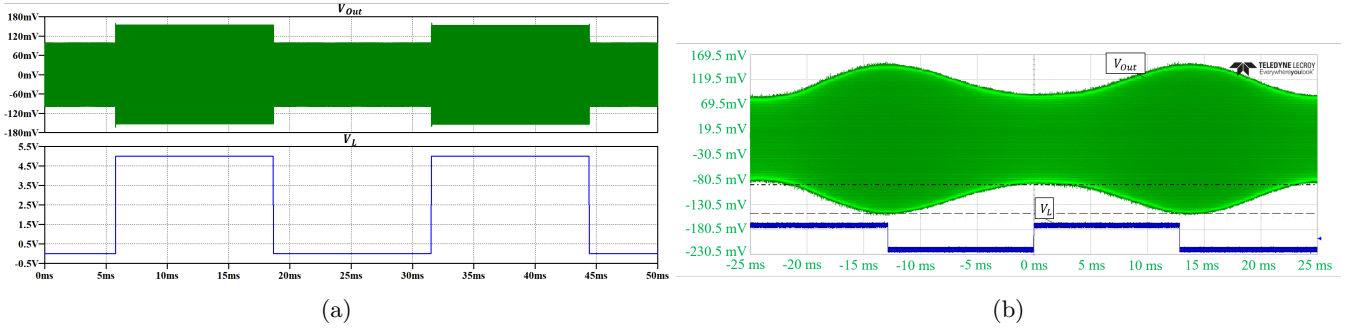


FIG. 9: Periodic variation of C_{DUT} leads to a periodic envelope at frequency f_L on top of the output signal at the carrier frequency $f_{DUT} = 222.1\text{kHz}$: (a) simulation results, and (b) oscilloscope data.

first harmonic f_1^{theory} , the cantilever can be thought of as being forced to displace below its mean position using a constant external force for 3.33 s and then left to oscillate freely back to equilibrium by “switching off” the force for 6.67 s. The envelope of the time domain data gives the damping time constant $\tau = 2.16\text{ s} = 1/\Gamma$ as shown in the inset to Fig. 8a (Eq. (A7)). The discrete Fourier transform of the measured data (Fig. 8b) shows clear peaking at $\simeq f_0 \pm 39\text{ Hz}$ and $\simeq f_0 \pm 193\text{ Hz}$, besides the carrier frequency $f_0 = 222.1\text{ kHz}$. These correspond to the flexural harmonics f_1 and f_2 . We also see peaks at $\simeq f_0 \pm 50\text{ Hz}$ and $\simeq f_0 \pm 100\text{ Hz}$ due to the 50 Hz line frequency noise.

B. Resonant drive to measure radiation force

When the cantilever is excited at its natural frequency **38.881 Hz** we see resonant oscillations (Fig. 10a). This frequency is found by tuning f_L around 39 Hz in fine steps until the maximum amplitude resonant signal is observed and is in agreement with the theoretical estimate (Eq. (6)).

The change in the DUT capacitance (ΔC_{DUT}) in this case can be obtained by matching simulations and experimental data shown in Fig. 9a and Fig. 9b respectively. The ΔV_{Out} signal envelope variation $53 \pm 5\text{ mV}$ (Fig. 10a) is reproduced in simulations when $\Delta C_{DUT} = 2.55 \pm 0.2\text{ fF}$ (Fig. 5). Then the Fourier amplitude of driving force F_0 at frequency $f_1 = 38.881\text{ Hz}$ is (Appendix A):

$$F_{Rad} = \frac{\pi}{4} \frac{\Delta C_{DUT}}{C_{DUT}} \frac{\mu L_C \Gamma \omega_1 w_0}{2\mathcal{I}} = \mathbf{1.438 \pm 0.323\text{ nN}}. \quad (7)$$

Here, $\mu = \rho A$ is the linear mass density, $w_0 = 0.43 \pm 0.02\text{ mm}$ is the mean steady-state separation between the two plates of the air capacitor, and \mathcal{I} is a dimensionless number derived in Appendix A. The $\pi/4$ pre-factor comes from the Fourier expansion of the square digital light

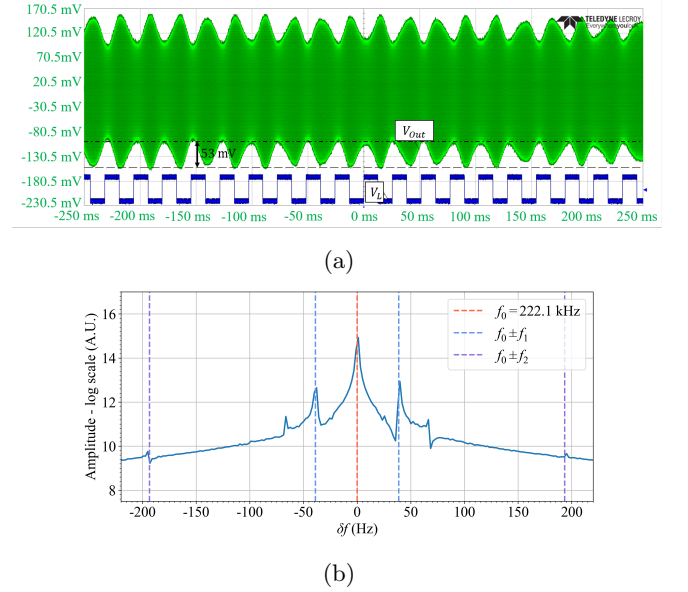


FIG. 10: Cantilever response for a resonant excitation at $f_L = f_1 = 38.881\text{ Hz}$: (a) oscilloscope data, and (b) discrete Fourier transform of the data.

pulse with force exerted switching between 0 and $2F_{Rad}$:

$$F(t) = F_{Rad} \left(1 + \frac{4}{\pi} \sin(\omega_1 t) + \frac{4}{3\pi} \sin(3\omega_1 t) + \dots \right). \quad (8)$$

For brass ($a+2r = 1.62$), this is equivalent to an RMS optical power P_{RMS} given by:

$$P_{RMS} = \sqrt{2} \left(\frac{cF_{Rad}}{1.62} \right) = \mathbf{0.377 \pm 0.085\text{ W}} \quad (9)$$

This agrees with the directly measured value (see Section III A) within error bounds.

We also observe resonant oscillations of the cantilever when excited at the second harmonic frequency $f_L = f_2 = 193.361\text{ Hz}$ (Fig. 11). This deviates from the theoretical second harmonic frequency, which can be attributed to non-idealities due to heating and size non-

uniformities that become significant for higher harmonics.

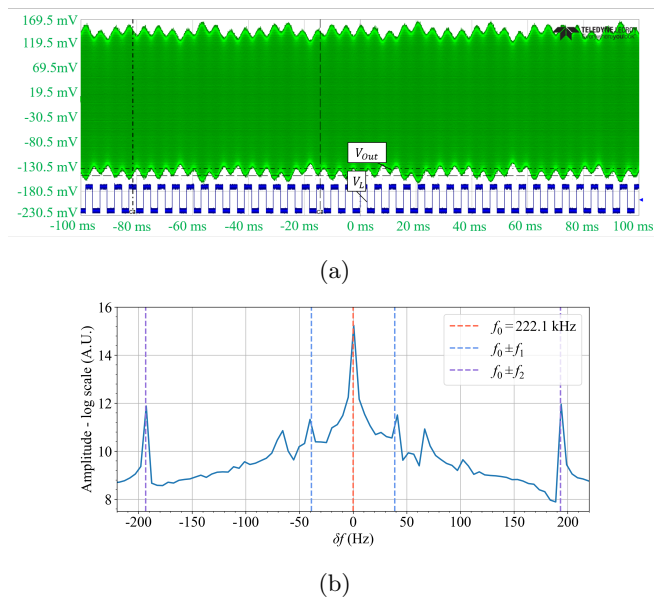


FIG. 11: Cantilever response for a resonant excitation at $f_L = f_2 = 193.361$ Hz: (a) oscilloscope data, and (b) discrete Fourier transform of the data.

This work demonstrates unambiguous detection of the mechanical vibrations of a thin metal cantilever caused by the radiation force, allowing detection of $\mathcal{O}(\text{fF})$ capacitance changes correlated to $\mathcal{O}(\text{nN})$ radiation forces. The experiment can be performed in ambient air conditions in a closed chamber, thus providing an accessible measurement of an otherwise hard-to-grasp theoretical aspect of Maxwell's equations.

ACKNOWLEDGEMENTS

We would like to thank the Instrumentation and Electronics Laboratory in the Department of Physics at the Indian Institute of Technology Bombay for the access to equipment and resources for this work.

AUTHOR CONTRIBUTION STATEMENT AND DATA AVAILABILITY

The authors declare no conflict of interest. **Devashish Shah**: Formal Analysis (lead); Investigation (lead); Conceptualization (equal); Writing – original draft (lead); Writing – review and editing (equal). **Pradumn Kumar**: Conceptualization (equal); Investigation (supporting). **Pradeep Sarin**: Supervision (lead); Conceptualization (equal); Writing – original draft (supporting); Writing – review and editing (equal).

The data supporting the conclusions is available from the corresponding author upon reasonable request.

Appendix A: DYNAMICS OF A DAMPED DRIVEN CANTILEVER^{11–13}

No external drive: The deflection of the cantilever $\Psi(x, t)$, from its mean position in the absence of an external drive and damping is given by:

$$\left(\frac{EI}{\rho A}\right) \frac{\partial^4 \Psi}{\partial x^4} + \frac{\partial^2 \Psi}{\partial t^2} = 0. \quad (\text{A1})$$

Separation of variables $\Psi(x, t) = \chi(x)\xi(t)$ can be used to rewrite Eq. (A1) as:

$$\left(\frac{EI}{\rho A \chi}\right) \frac{d^4 \chi}{dx^4} = -\frac{1}{\xi} \frac{d^2 \xi}{dt^2} = \omega^2, \quad (\text{A2})$$

where ω^2 is a constant. The general solution to the above equation can be written as a superposition of its free vibration eigenmodes $\phi_n(x)$:

$$\Psi(x, t) = \sum_{n=1}^{\infty} \phi_n(x) (A_n \sin(\omega_n t) + B_n \cos(\omega_n t)). \quad (\text{A3})$$

Applying appropriate boundary conditions, the flexural eigenmodes can be shown to be:

$$\phi_n(x) = \cos(\beta_n x) - \cosh(\beta_n x) - \kappa_n (\sin(\beta_n x) - \sinh(\beta_n x)), \quad (\text{A4})$$

where, $\beta_n^4 = \mu \omega_n^2 / EI$, $\kappa_n = (\cos(\beta_n L_C) + \cosh(\beta_n L_C)) / (\sin(\beta_n L_C) + \sinh(\beta_n L_C))$, and $\beta_1 L_C = 1.875$, $\beta_2 L_C = 4.694$, $\beta_3 L_C = 7.855$. Here, $\mu = \rho A = \rho b h$ is the linear mass density. ϕ_n are orthogonal, with:

$$\int_0^{L_C} \phi_n \phi_m dx = L_C \delta_{nm} \quad (\text{A5})$$

In the presence of damping, the equation of motion is:

$$\left(\frac{EI}{\rho A}\right) \frac{\partial^4 \Psi}{\partial x^4} + \frac{\partial^2 \Psi}{\partial t^2} + \gamma \frac{\partial \Psi}{\partial t} = 0. \quad (\text{A6})$$

Using a similar procedure as before, χ is spanned by $\phi_n(x)$ and for $\xi(t) = e^{i\alpha_n t}$, we have:

$$\alpha_n = i \frac{\gamma}{2} \pm \omega_n \sqrt{1 + \frac{\gamma^2}{4\omega_n^2}}. \quad (\text{A7})$$

Thus, for a cantilever deflected from its mean and left to oscillate, the oscillations decay exponentially as $e^{-\gamma t/2}$, which can be measured experimentally ($\Gamma = \gamma/2$).

Sinusoidal drive - radiation force: In the presence of an external sinusoidal force applied at the tip of the cantilever, the motion of the cantilever is governed by:

$$\left(\frac{EI}{\rho A}\right) \frac{\partial^4 \Psi}{\partial x^4} + \frac{\partial^2 \Psi}{\partial t^2} + \gamma \frac{\partial \Psi}{\partial t} = \frac{F_1}{\rho A} \delta(x - L_C) e^{i\Omega t}. \quad (\text{A8})$$

For an under-damped oscillator in steady state, $\Psi(x, t) = \sum_n A_n \phi_n(x) e^{i\omega_n t}$. When driven at resonance $\Omega = \omega_1$:

$$|A_1| = \frac{F_1}{\Gamma \omega_1 \mu L_C}. \quad (\text{A9})$$

Thus, the maximum deflection of the cantilever from its mean position is $\Delta(x) = |A_1| |\phi_1(x)|$. Here, ϕ_1 is dimensionless, and A_1 has the dimension of length. The capacitance of the air capacitor when the cantilever is displaced to one of the extremes is $C'_{DUT} = C_{DUT} \pm \Delta C_{DUT}/2$.

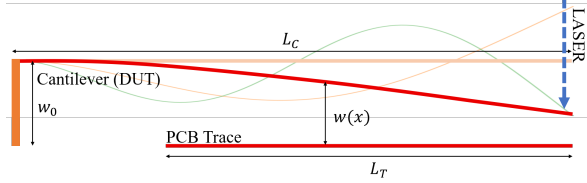


FIG. 12: The change in capacitance of the deflected cantilever is dominated by the first flexural eigenmode. This is the case when the beam is pulsed at $f_1 = 38.881\text{Hz}$.

For small deflections, the maximum change in the capacitance is:

$$\frac{\Delta C_{DUT}}{2} = 2\epsilon_0 \frac{A_C A_T}{A_C + A_T} \int_{L_C-L_T}^{L_C} \frac{|\Delta(x)| dx}{w_0^2 L_C}. \quad (\text{A10})$$

Here $A_C = bL_C$ and $A_T = bL_T$ are the areas of the cantilever plate and the PCB trace, respectively, with L_T

being the length of the PCB trace. For our setup, $L_T = 1.900 \pm 0.002$ cm. Integration is over the region of overlap, with $x = 0$ being the suspension point. The factor of half on the LHS is because experimentally, we determine the peak-to-peak value of the change in capacitance denoted as ΔC_{DUT} . Using the expression for $\Delta(x)$ we get:

$$\frac{\Delta C_{DUT}}{2} = \frac{C_{DUT} |A_1|}{w_0} \int_{L_C-L_T}^{L_C} \frac{|\phi_1(x)|}{L_C} dx. \quad (\text{A11})$$

All quantities in the above expression can be measured or obtained via simulation, allowing us to calculate the force amplitude F_1 (using A9):

$$F_1 = \left(\frac{\Delta C_{DUT}}{C_{DUT}} \right) \frac{\mu L_C \Gamma \omega_1 w_0}{2\mathcal{I}}. \quad (\text{A12})$$

Here, \mathcal{I} is the dimensionless integral in Eq. (A11). Further, the absolute maximum error in measurement can be estimated by accounting for relative errors in all quantities in Eq. (A12):

$$\begin{aligned} \frac{\delta F_1}{F_1} &= \frac{\delta \Delta C_{DUT}}{\Delta C_{DUT}} + \frac{\delta C_{DUT}}{C_{DUT}} + \frac{\delta \rho}{\rho} \\ &+ \frac{\delta A}{A} + \frac{\delta L_C}{L_C} + \frac{\delta w_0}{w_0} + \frac{\delta \mathcal{I}}{\mathcal{I}}. \end{aligned} \quad (\text{A13})$$

The relative errors in determining ω_1 and Γ are negligible compared to relative errors in measurement of L_C , w_0 , A , and ρ due to the resolution of the caliper and uncertainty in E . The error in calculating \mathcal{I} propagates from errors in L_C and L_T .

* devashish_shah@iitb.ac.in

- ¹ S. G. Brush, C. W. F. Everitt, “Maxwell, Osborne Reynolds, and the radiometer,” *Historical Studies in the Physical Sciences*, Vol.1: 105–125, (1969).
- ² P.N. Lebedev, “Experimental examination of light pressure,” *Journal of Russian Physicochemical Society*, 33(1), 53–75 (1901).
- ³ Dakang Ma, Joseph L Garrett, Jeremy Munday, “Quantitative measurement of radiation pressure on a microcantilever in ambient environment” *Appl. Phys. Lett.*; 106 (9): 091107 (2015)
- ⁴ J. A. Boales, F. Mateen, P. Mohanty, “Micromechanical Resonator Driven by Radiation Pressure Force,” *Sci Rep* 7, 16056 (2017)
- ⁵ M. Partanen, H. Lee, K. Oh, “Radiation pressure measurement using a macroscopic oscillator in an ambient environment,” *Sci Rep* 10, 20419 (2020).
- ⁶ D. J. Griffiths, *Introduction to Electrodynamics*, 4th Ed. (Cambridge University Press, Cambridge, 2013), pp. 398–400.
- ⁷ D. Ma, J.N. Munday. “Measurement of wavelength-

- dependent radiation pressure from photon reflection and absorption due to thin film interference” *Sci Rep* 8, 15930 (2018).
- ⁸ LF411C JFET Op-Amp, Texas Instruments, <https://www.ti.com/product/LF411>.
- ⁹ LTSpice circuit simulator, Analog Devices, <https://www.analog.com/en/resources/design-tools-and-calculators/ltspice-simulator.html>
- ¹⁰ A. Passian, A. Wig, F. Meriaudeau, T. L. Ferrell, and T. Thundat. Knudsen forces on microcantilevers. *Journal of Applied Physics*, 92(10):6326–6333, 2002.
- ¹¹ C. E. Repetto, A. Roatta, R. J. Welti, “Forced vibrations of a cantilever beam” *Eur. J. Phys.* 33 1187 (2012).
- ¹² A.W. Leissa, M.I. Sonalla “Vibrations of cantilever beams with various initial conditions” *Journal of Sound and Vibration*, Volume 150, Issue 1 (1991).
- ¹³ M. Romaszko, B. Sapiński, A. Sioma, “Forced vibrations analysis of a cantilever beam using the vision method,” *Journal of Theoretical and Applied Mechanics*, 53(1), 243–254 (2015).